Estimation of the heat source parameters during the deposition of SS316L wire with GMAW-CMT process: application to additive manufacturing.

Camille CAMBON, Sébastien ROUQUETTE*, Issam BENDAOUD, Fabien SOULIÉ

LMGC, Univ. Montpellier, CNRS, Montpellier, France.
(*Corresponding author : sebastien.rouquette@umontpellier.fr)

Abstract: A wire and arc additive manufacturing process is presented. The heat source used to melt the stainless steel 316L wire is provided with a CMT-GMAW generator. A heat transfer modelling and simulation of the deposition is presented. The heat source is modelled with a double ellipsoid. Two parameters of the heat source require to be estimated. These parameters have been estimated to 0.671 for the GMAW efficiency and 2.1 mm for the Gaussian distribution. The calculated temperature field will be used for further mechanical computations in the aim to get the residual stress field.

Keywords: wire and arc additive manufacturing; Gas Metal Arc Welding; heat transfer modeling; Levenberg-Marquardt.

Nomenclature

e thickness [m]
R^3 Euclidian space
$\vec{x}$ vector
t time variable [s]
$T_{(\vec{x},t)}$ temperature [K]
$C_p(T)$ Specific heat [J.kg^{-1}.K^{-1}]
$h_{(T)}$ Convective heat transfer coefficient [W.m^{-2}.K^{-1}]
I welding current [A]
U welding tension [V]
a, b semi-axis of 2D ellipsoid
Greek symbols
Ω geometrical domain
$\rho_{(T)}$ Mass density [kg.m^{-3}]
λ_T Heat conductivity [W.m^{-1}.K^{-1}]
∂ Partial derivative
ϵ Coefficient of emissivity
σ Stefan's constant [W.m^{-2}.K^{-4}]
η Efficiency of welding process

1 Wire and arc Additive manufacturing challenges

Wire + Arc Additive Manufacturing (WAAM) process allows producing metallic parts by melting a wire given with an electric heat source and stacking up the deposits one after the other vertically. The Additive Manufacturing (AM) processes are a promising alternative to traditional subtractive machining processes. The advantages are complex and/or large geometries, raw material savings, cheap industrial plant, straightforward health and safety matter, high deposition rate (~300 cm³/h) in comparison to other AM processes using metallic powders (such as Selective Laser Melting or Electron Beam Melting ones with deposition rates up to 15 cm^3/h) [1,2]. Nevertheless WAAM parts present high level of tensile residual stresses and inherent distortions inherent due to the process used to melt the wire especially with Gas Metal Arc Welding (GMAW) sources [3]. Mechanical properties and life cycle of Wire + Arc Additive Manufacturing parts rely on their induced residual stresses. Post manufacturing heat or mechanical treatments are currently investigated for reducing the tensile stresses [4]. Distortions and residual stresses are affected by the process parameters such as deposition energy (U, I), deposition speed, deposition pattern… We are investigating the effect of these process parameters (deposition speed and energy) on the final residual

https://doi.org/10.25855/SFT2020-128

stress field and distortions by carrying out both numerical and experimental approaches. The experimental approach consists in a simplified case for getting measurements such as electric signals (U, I), local temperatures, local displacement and images of deposition with high speed camera. These measurements are used for validating the numerical approach. The numerical study consists in a thermo-mechanical simulation of the experimental case in order to get the residual stress field. In this communication, the thermal problem is only considered as the solution of the mechanical problem relies totally on the accuracy of the thermal one.

Thermal modelling and simulation of arc welding processes have been extensively studied since the theory of moving heat sources of Rosenthal in 1946 [5]. Nowadays, it is common to perform complex simulations of arc welding such as GMAW one including fluid flow and electro-magnetics or mechanics and metallurgy [6,7]. Furthermore, the geometry of the deposit can be considered totally at the beginning of the simulation [7] or resized at each time step [8]. In this work, we focused on the thermal problem in order to compute accurately the temperature field before using it in the mechanical simulation. The heating is due to the electric arc and this one is modeled with a double ellipsoid expression in the thermal problem [9]. As the power input is known (U, I), two heat source parameters require to be estimated: process efficiency and Gaussian distribution. These two parameters are estimated by solving an inverse heat transfer problem regularized with Levenberg-Marquardt method [10]. Firstly, we define the studied experimental case. Then the considered geometry and the thermal modeling are presented. The inverse heat transfer problem is stated and solved with numerical tests in order to prove its robustness and reliability. Then the two heat source parameters are estimated from one set of measured temperatures.

2 Wire and arc Additive manufacturing facility

The Wire + Arc Additive Manufacturing facility consists of a Fronius CMT-GMA Welding generator with its welding torch fitted onto a six axis KUKA robot (1 in Figure 1). The CMT-GMAW is used to drive the wire and melt it. The Additive Manufactured samples are made by overlaying a new deposit upon the previous one as drawn in Figure 2. The Additive Manufactured samples are deposited on a base plate (2 in Figure 1) made of same material as the wire: Stainless Steel 316L (SS316L).

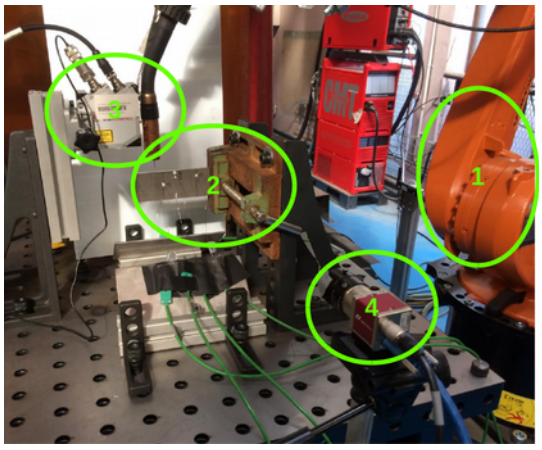

Figure 1 : *WAAM equipment suited with acquisition systems.*

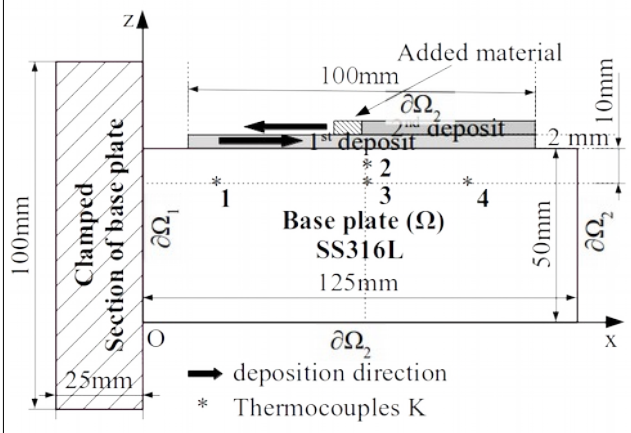

Figure 2 : *schematization of base plate and overlaid deposits.*

The deposition procedure is monitored in real time: electric signals are recorded at 30 kHz frequency as presented in Figure 3. Five type K thermocouples, 0.5 mm diameter, are inserted 2 mm into the base plate at a 20 Hz frequency, a laser sensor (3 in Figure 1) measures the displacement of the base plate extremity (x = 125 mm) and a speed camera records the weld pool zone (4 in Figure 1). The electric signals, displayed in Figure 3, are a feature of Cold

Metal Transfer – Gas Metal Arc Welding allowing melting metal at low energy. The averaged experimental values are $\widetilde{U}$ = 11.8 V and $\widetilde{I}$ = 106.5 A.

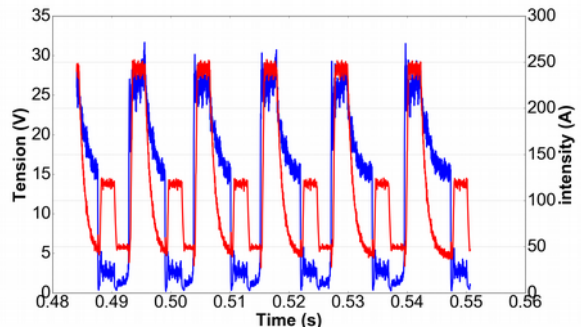

Figure 3 : *sample of welding tension and intensity (respectively in blue and red).*

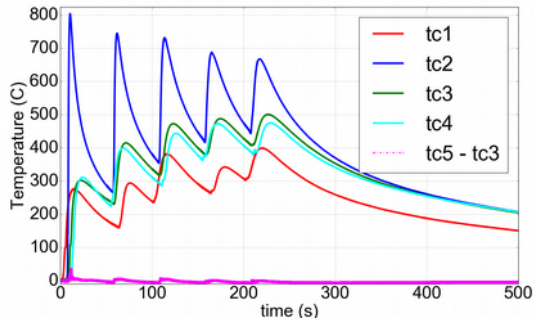

Figure 4 : *measured temperatures for 5 overlaid deposits.*

The temperature is measured at 5 different locations of the base plate as shown in Figure 2. The time evolution of the temperatures presents 5 peaks corresponding to the 5 deposition passes. A pause of about 35s is realised between each passes. Let's remark, that thermocouples n°3 and 5 were positioned at the same vertical and horizontal location but on opposite sides of the base plate. The curves match quite well as shown in Figure 4 by plotting the difference between tc5 and tc3. This result confirms the assumption of thin plate for the heat transfer modelling. During the 1st deposition, the heating rate is about 302 K/s and the cooling is -30 K/s. After the 5 deposits, the cooling rate is -1.3 K/s between 300 s and 500 s.

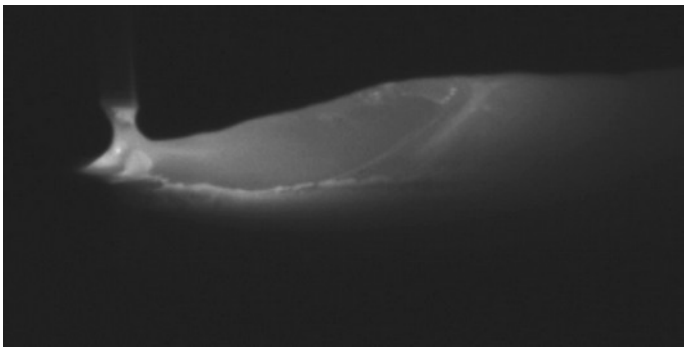

Figure 5 : *view of the weld pool during the 1st deposit with a SS316L wire of 1.2 mm diameter.*

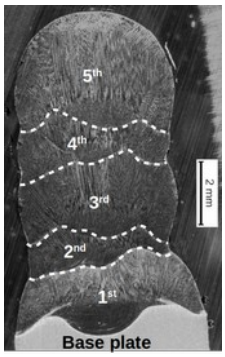

Figure 6 : *macrography of the 5 deposits realized at x ~ 64 mm.*

The weld pool length and penetration have been estimated from Figures 5 and 6. The weld pool length was 11-12 mm and the penetration was 1.2 mm. The width of the 5 deposits is about 5 mm, see Figure 6. The 5 passes are clearly visible on the macrography. The passes 1, 3 et 5 were made in the (Ox) direction while 2 and 4 were done in the opposite direction to (Ox). It is noticed that passes 2 & 4 are almost remelted by the next one. This behavior has been observed on two other macrographies done at x ~ 45 mm and 89 mm. The length of each deposit varied in the range 103-105 mm.

In what follows, we are focusing on the heat transfer modelling of the 1st deposit in the time interval [0 s; 50 s]. An accurate simulation of the heat transfer of this experiment is necessary as the thermal field is used in a mechanical simulation in order to calculate the residual stresses in AM sample.

3 Heat transfer modelling and finite elements analysis

Let's define the studied domain without the clamped section (hatched one) as depicted in Figure 2. The BP sizes are 125 x 50 x 6 mm^3 . A 2D study is carried out as the thickness is

smaller than the others dimensions. The BP and 1.2 mm wire are made of SS316L. The height of the deposits was varying between 1.9-2.0 mm height. Then, a 2 mm height is used.

Let's define firstly the heat conduction equation with a heat source term:

$$\rho C_p^{eq}.\frac{\partial(T)}{\partial t}-\nabla.(\lambda\nabla T)=Q_{(\vec{x},t)}-\frac{h}{e}(T-T_{amb})+\frac{\varepsilon\sigma}{e}(T^4-T_{amb}^4) \quad \text{in} \quad \Omega x I \qquad (1)$$

with $\vec{x}=(x,z)$ and $\vec{x}\in\Omega$, I is the time interval and $T=T(\vec{x},t)$ is the temperature field. $Q(\vec{x},t)$ is a volume heat source describing the absorbed electric energy by the BP and deposit. ρ, C_p^{eq} et λ are respectively the density, the specific heat and the heat conductivity of SS316L [9], they are temperature dependent. Radiative and convective losses on the lateral sides are taken into account in (1).

Two boundary conditions are associated to (1):

$$-\lambda(\frac{\partial T}{\partial \vec{n}}).\vec{n}=R_{clamp}(T-T_{amb}) \quad \text{on} \quad \partial\Omega_1 x I \qquad (2)$$

with an estimated thermal contact resistance R_{clamp} due to the clamped section of BP.

$$-\lambda(\frac{\partial T}{\partial \vec{n}}).\vec{n}=h(T-T_{amb})+\varepsilon\sigma(T^4-T_{amb}^4) \quad \text{on} \quad \partial\Omega_2 x I \qquad (3)$$

where h is the coefficient of convective exchange set to 15 W/m/°C and ε is the emissivity of SS316L set to 0,5. The initial condition is set equal to the laboratory ambient temperature:

$$T_{(\vec{x},t=0s)}=T_{amb}\approx 293K \qquad (4)$$

The volumetric heat source expression is described with a double ellipsoid as proposed by Goldak [10]. Its expression is modified for 2D purpose as:

$$Q_{(\vec{x},t)}=\frac{3.\eta.\tilde{U}.\tilde{I}.f_i}{a.b.\pi.e}e^{-3\frac{[x+v(\tau-t)]^2}{a^2}}e^{-3\frac{z^2}{b^2}} \qquad (5)$$

with f_i is shape factor [10]. In front of the heat source, $f_i=f_{front}=0.4$ and at the rear $f_i=f_{rear}=1.6$ such as $f_f+f_r=2$ and $f_f/a_f=f_r/a_r$. This last relation is required for some mathematical continuity purpose so $f_f=2a_f/(a_f+a_r)=2-f_r$. a_i and b are the Gaussian distribution parameters of (5) knowing that $a_f=b/2$ and $a_r=2.b$. e is the base plate thickness that is equal to 6 mm.

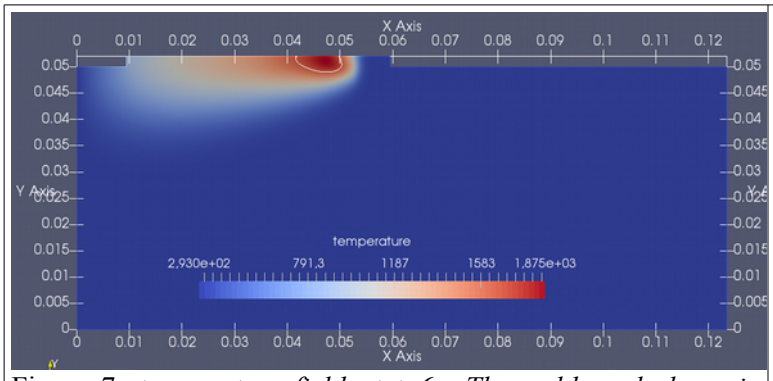

Figure 7: *temperature field at t~6s. The weld pool shape is given with the white line (T=1653 K).*

Figure 7 presents the temperature field calculated at t~6s. The calculated weld pool length is about 9.5 mm against 11-12 mm from Figure 5. The weld pool penetration is about 1mm. The maximum temperature is reached in the weld pool with 1875 K. Most of the base plate is not yet affected thermally.

parameter	$\tilde{I}$ (A)	$\tilde{U}$ (V)	V_S (mm/s)	η	b (mm)	δt (s)	δx ** (mm)	h (W/m/K)
Valeur	106.5 (119*)	11.8 (13.5*)	7	0.75	3.7	0.05	0.4	25

Table 1 : *main parameters used in the simulation.* values given by the manufacturer. ** minimum space size used in the deposit and 3 mm under it.*

The set of equations (1) to (5) is solved with a finite element analysis. The free software Elmer CSC has been used ((https://www.csc.fi/web/elmer). The values of the different parameters used in the simulation are shown in Table 1. The deposit length is divided into 10 sub-deposits which are activated along the simulation. A python program manage the transfer of the temperature field between the geometries (for the update the deposit length). The previous temperature field is projected on the new mesh as initial temperature condition.

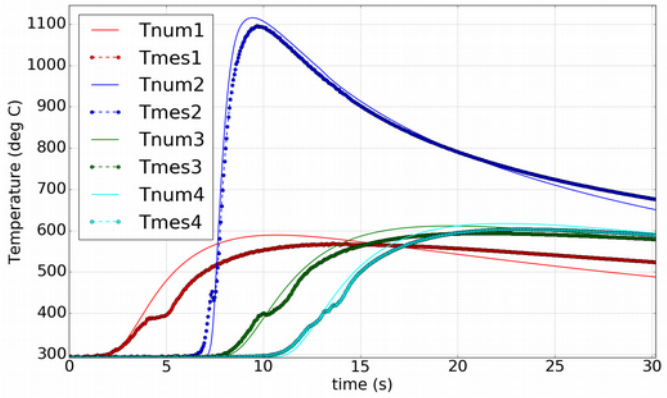

Figure 8: *comparison between numerical and measured temperatures at 4 points.*

Some discrepancies are noticed between the calculated and measured temperatures, see Figure 8. This is mainly due to the inaccurate knowledge of the two heat source parameters η and b. Indeed, other sources of errors such as weak thermal contact between thermocouples and base plate, accuracy of thermophysical properties introduce some differences between the numerical and experimental temperatures.

In the next section, an inverse problem is stated in order to estimate the two unknown parameters of the heat source: Gas Metal Arc Welding efficiency η and Gaussian distribution b.

4 Inverse heat transfer problem and numerical resolution

4.1 Inverse heat transfer formulation

The IHTP general formulation is written as:

Find the unknown vector $\bar{p}=\{\eta, b\}$ such that the measured temperatures $Y_{mes}(t)$ equal the calculated temperatures $T_{num}(\vec{x},t)$ at each sensors located at point x_i with $i=1,\ldots,n_S$ and for any time steps t_j with $j=1,\ldots,n_t$

Let's introduce a quadratic criterion (or also called objective function) [10]:

$$S(\bar{p})=\frac{1}{2}[Y_i-T_i]^T W[Y_i-T_i] \quad (6)$$

Thus, a second formulation of the inverse problem is stated:

Find the vector $\bar{p}=\{\eta, b\}$ which minimizes the cost function $S(\bar{p})$

4.2 Sensitivity analysis

Details of this method are given in [10]. Only some key points of this method are presented hereafter. The Levenberg-Marquardt method is associated to an iterative procedure and the unknown vector $\bar{p}=\{\eta, b\}$ is computed after each iteration $k+1$ as follows:

$$\bar{p^{k+1}}=\bar{p^k}+[(J^k)^T W J^k+\mu^k \Omega^k]^{-1}[(J^k)^T W(T_i(\bar{p^k})-Y_i)] \quad (7)$$

with $J(\bar{p})$ is the sensitivity matrix which is defined as the transpose of the term $\partial T_i(\bar{p})/\partial p$. The elements of the sensitivity matrix are called the sensitivity coefficients. The sensitivity coefficients are the first derivative of the estimated temperature with respect to the unknown parameters $\bar{p}=\{\eta, b\}$. μ^k is a positive scalar which is introduced to prevent that the matrix $J^T J \approx 0$ is ill-conditionned near the initial guess. Ω^k is a diagonal

matrix. The damping parameter μ^k is large at the beginning of the iterative procedure (and the method is like the steepest descent method) then it decreases when the procedure progresses to the solution (and the method tends to the Gauss method). W is a diagonal matrix where its diagonal elements are given by the inverse of the standard deviation of the measurement errors.

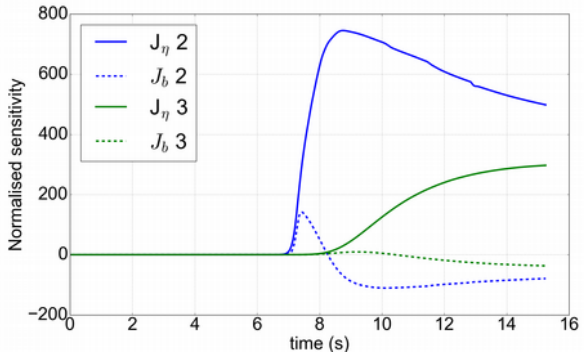

Figure 9: *evolution of the normalised sensitivity coefficients at sensors 2 and 3 for η and b.*

A sensitivity study has been carried out in order to determine when the measured temperatures Y_i (according to each sensor) are relevant for the estimation procedure. Each parameter of $\bar{p}=\{\eta, b\}$ have been analysed. A finite difference scheme has been used to determine the sensitivity coefficients. The sensitivity coefficients of efficiency parameter η are obtained as follows : $J_i(\eta)=\frac{T_i(\eta+\epsilon)-T_i(\eta-\epsilon)}{2\epsilon}$.

The evolution of the normalised sensitivity (e.g. $\eta.J_i(\eta)$) is displayed in Figure 9 for 2 sensors only. Obviously, the sensitivity remains null till the sensor is subjected to the heating so from times greater then 7 s for sensor 2 (8 s for sensor 3). The normalised sensitivity of parameter b is about 5 times lower than the one of parameter η. The parameter b will be more difficult to estimate accurately. The sensitivity of both parameters is almost constant, with time, after t>11s so data after this time are not really relevant for the estimation. Finally, the useful time interval at sensor 2 is defined between 7 s and 12 s. The same analysis was performed at the 3 other sensors. These results are summarized in Table 2. The time interval of the simulation is also limited to 15s as further data is not relevant.

	Thermocouple 1	Thermocouple 2	Thermocouple 3	Thermocouple 4
Position (mm)	(19.5; 40)	(61.5 ; 46.5)	(61.3 ; 39.5)	(81.5 ; 39.8)
Time interval (s)	~ 2-7	~ 7-12	~ 8-14	~ 11 -15

Table 2 : *position of 4 thermocouples and relevant time interval for the estimation.*

4.3 Numerical tests

Three numerical tests have been performed in order to validate the inverse procedure. The cases 1 & 2 were initialized with different initial guess for $\bar{p}=\{\eta, b\}$ while the 3rd case used noised input data (3% of exact input temperature used for cases 1 & 2) The exact input data were obtained from a simulation with $\eta=0.85$ and $b=3.6$ mm). The results are presented in Table 3.

	Quad. criterion initial / final	Standard deviation ±σ	Efficiency initial /final	b (mm) initial / final
Case 1	$5.39\text{x}10^{5}$ / $3.6\text{x}10^{-3}$	0	0.99 / 0.85	1.35 / 3.6
Case 2	$6.63\text{x}10^{6}$ / $3.1\text{x}10^{-3}$	0	0.1 / 0.85	10 / 3.6
Case 3 (noised)	$1.72\text{x}10^{6}$ / $9.8\text{x}10^{3}$	10.8	0.5 / 0.8539	6 / 3.649

Table 3: *results of numerical test carried out in order to validate the inverse procedure.*

The 3 cases converged to the values $\eta=0.85$ and $b=3.6$ mm. The 3rd case converged to the exact values correctly with low errors on the two estimates (due to the noise added to

the exact input data). The error on the estimate of the efficiency is lower to 0.5% while the error on the estimate of Gaussian distribution is lower than 1.4%. This last parameter is the most difficult to estimate as a conclusion of the sensitivity analysis.

5 Estimation of the experimental heat source parameters

The measured temperatures at sensors 2, 3 and 4 were used. The data from sensor 1 prevented a realistic estimation of the two parameters. An investigation of the boundary condition applied on boundary $\partial\Omega_1$ with a thermal contact resistance (in order to replace the missing part of the base plate) led to inaccurate computed temperature at sensor 1. The comparison was done numerically with the real geometry of the baseplate. The convective exchange coefficient has been investigated as well with using values from 15 W/m/K to 150 W/m/K. The 15 W/m/K value led to better results during the cooling between 15s and 30s of measured temperature in Figure 8.

Performing the inverse problem with the 4 thermocouples led to unrealistic parameters for $\bar{p}=\{\eta, b\}$. The Gaussian distribution was especially affected with large value: about 4.mm. The efficiency was also higher. The calculated temperatures at sensors 1, 3 and 4 matched well the experimental ones while the calculated temperature at sensor 2 was totally underestimated. Furthermore, the maximum temperature into the deposit never overtook the melting temperature (1658 K).

	Quad. criterion initial / final	Average standard deviation ±σ	Efficiency initial /final	b (mm) initial / final
Experimental case	9.24e6 / 1.07e-5	28.1	0.4/ 0.671	7 / 2.1

Table 4: *results of the estimation with experimental data.*

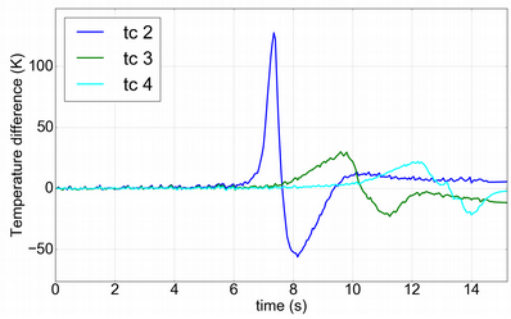

Figure 10: *evolution of temperature residual (Tmes – Tnum)(t).*

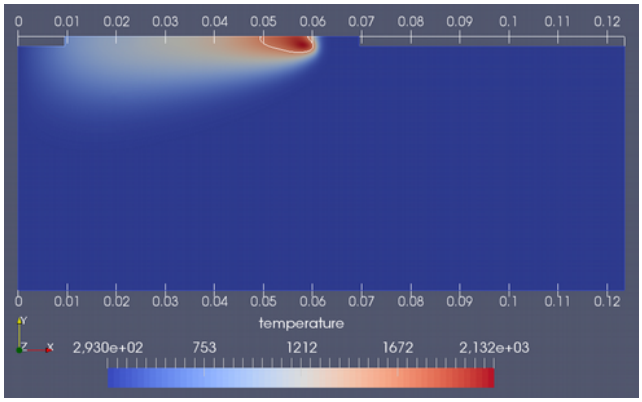

Figure 11 : *Calculated temperature field at t~7.3s.*

Thus, we used only sensors 2, 3 and 4 as they were far from this boundary. The results of the estimation done with sensors 2, 3 and 4 are presented in Table 4. The process efficiency and Gaussian distribution are estimated to 0.671 and 2.1 mm respectively. The average standard deviation is ±28 K. Nonetheless the maximum temperature residual, up to 120 K, is reached at sensor 2 as presented in Figure 10. The sensor 2 experienced the highest measured temperatures with a maximum of 1100K. Figure 11 displays the obtained temperature field. The weld pool sizes are 11 mm for its length and 1.3 mm for its penetration quite close to the ones observed experimentally.

6 Conclusions

In this communication, a wire and arc additive manufacturing process is presented. This process uses a specific gas metal arc welding generator: the Cold Metal Arc. This work is dedicated to the heat transfer analysis occurring during the deposition of molten SS316L wire. Several deposits are overlaid upon the last one. Thus, a heat transfer modelling is presented and a finite element analysis is done. As the calculated temperatures do not match the experimental ones, an inverse heat transfer problem is stated and solved. Two parameters are estimated: the welding process efficiency was evaluated to 0.671 and a Gaussian distribution b was assessed to 2.1 mm. During this inverse procedure, it appeared that temperature from one sensor prevented any realistic estimates. The problem is due to a wrong boundary conditions used to model the clamping part of the base plate.

The final aim of this work is to use the calculated temperature field into a mechanical computation in order to predict the final distortions and residual stresses of the sample.

References

[1] I. Tabernero, A. Paskual, P. Álvarez, A. Suárez , Study on Arc Welding processes for High Deposition Rate Additive Manufacturing, *Procedia CIRP* 68, (2018) 358–362.

[2] D. Ding, Z. Pan, D. Cuiuri, H. Li, Wire-feed additive manufacturing of metal components: technologies, developments and future interests, *Int. J. Adv. Manuf. Technol*, 81, (2015) 465-481.

[3] P. Colegrove, C. Ikeagu, A. Thistlethwaite, S. Williams, T. Nagy, W. Suder, A. Steuwer and T. Pirling, Welding process impact on residual stress and distortion, *Science and Technology of Welding and Joining*, 14, (2009) 717-725.

[4] F. Martina, M. Roy, B. Szost, S. Terzi, P. Colegrove, S. Williams, P. Withers, J. Meyer & M. Hofmann, Residual stress of as-deposited and rolled wire + arc additive manufacturing Ti–6Al–4V components, *Materials Science and Technology*, 32, (2016) 1439-1448.

[5] D. Rosenthal, The theory of moving sources of heat and its application to metal treatments, *Transations of ASME*, (1946) 849:866.

[6] J. Hu, H.L. Tsai, Heat and mass transfer in gas metal arc welding. Part I: The arc, *Int. J. of Heat and Mass Transfer* 50, (2007) 833-846.

[7] H.P. Manurung, N. Lidam, R. Rahim, Y. Zakaria, R. Redza, S. Sulaiman, G. Tham, Welding distortion analysis of multipass joint combination with different sequences using 3D FEM and experiment, *International Journal of Pressure Vessels and Piping* 111, (2013) 89-98.

[8] J. Ding, P. Colegrove, J. Mehnen, S. Ganguly, P.M. Sequeira Almeida, F. Wang, and S. Williams, Thermo-mechanical analysis of Wire and Arc Additive Layer Manufacturing process on large multi-layer parts, *Computational Materials Science* 50, (2011) 3315-3322.

[9] K.C. Mills. *Recommended values of thermophysical properties for selected commercial alloys*, Woodhead Publishing Series in Metals and Surface Engineering (2002).

[10] J. Goldak, A. Chakraverti, M. Bibby. A new finite element model for welding heat sources, *Metallurgical Transations B*, 15B, (1984) 299-305.

[11] Ozisik N. M., and Helcio R. B. Orlande, *Inverse heat transfer fundamentals and applications*, *Taylor and Francis, New York (*2000).